

High p_T Measurements from PHENIX

S. Mioduszewski^a for the PHENIX Collaboration*

^aPhysics Department, Brookhaven National Laboratory, Upton, NY 11973, USA

We present recent high transverse momentum measurements by the PHENIX experiment for Au+Au and p+p collisions at $\sqrt{s_{NN}} = 200$ GeV at the Relativistic Heavy Ion Collider (RHIC). We show particle spectra for neutral pions and charged hadrons, define and show the nuclear modification factor, and discuss particle composition. By means of the nuclear modification factor, we observe a suppression factor of 5-6 for neutral pions and 3-4 for charged hadrons in central collisions at high p_T . We find that the ratio of π^0 to $(h^+ + h^-)/2$ remains nearly constant at ~ 0.5 for $p_T = 2 - 9$ GeV/c. Finally we present strong evidence for the observation of jets in Au+Au collisions.

1. Introduction

In Run II at RHIC ($\sqrt{s_{NN}} = 200$ GeV), PHENIX has been able to measure particle yields up to large transverse momenta, $p_T \sim 10$ GeV/c, where the cross section is expected to be dominated by hard processes. This high statistics data set allows us to study the systematics of high p_T phenomena in detail and at much higher p_T than possible in Run I ($\sqrt{s_{NN}} = 130$ GeV) data.

In p+p collisions, it is known that hard scattering and the fragmentation of the scattered partons dominates the production of hadrons above $p_T \sim 2$ GeV/c [1]. In Au+Au collisions, these hard scatterings are of particular interest because they occur early in the collision, leaving the hard-scattered partons sensitive to the properties of the collision medium. Further interactions of these partons in the dense medium might cause the high transverse momentum tail of the hadron spectrum, where the hadrons are likely to be the leading particles of jets, to be suppressed [2]. Due to the high multiplicity environment, jets cannot be directly observed in a heavy ion collision. We can however determine the contribution of jet fragmentation to hadron yields at high p_T via correlation measurements and use this knowledge to interpret the measured hadron p_T spectra.

First, we give a brief overview of the PHENIX detector. In the following sections, we proceed assuming that the hadrons at high p_T emanate from jets, with the objective of measuring the effect of the dense medium on the hard-scattered partons through modification of the particle spectra at high p_T . We define the nuclear modification factor and show such a quantity for both neutral pions and charged hadrons. With the measurement of spectra for both charged hadrons and neutral pions, we also investigate the particle

*for the full PHENIX Collaboration author list and acknowledgements, see Appendix "Collaborations" of this volume.

composition at high p_T . Finally, we use two-particle correlations to test the assumption that the high p_T hadrons are due to the fragmentation of hard-scattered partons.

2. Overview of the PHENIX Detector

PHENIX is a versatile detector, with tracking chambers, ring-imaging Cerenkov (RICH) detectors, a time-of-flight (TOF) wall, and electromagnetic calorimeters in the central arms, which cover $\Delta\eta = \pm 0.35$ and 180° in azimuth. Along the beamline there are beam-beam counters and zero-degree calorimeters, which are used for event triggering and centrality classification. Neutral pions are measured via their $\gamma\gamma$ -decay using the electromagnetic calorimeters (EMCal). There are 6 sectors of Lead-Scintillator (PbSc) and 2 sectors of Lead-Glass (PbGl) calorimeter, providing two independent measurements of the π^0 p_T spectrum. The charged hadron spectrum is measured using the tracking detectors: drift chambers and pad chambers. At p_T above ~ 5 GeV/c the RICH detector, together with an energy cut in the PbSc, is used to identify charged pions. With various detection methods, PHENIX can make multiple overlapping measurements at high p_T , providing valuable consistency checks. Details of the detector are described elsewhere [3].

3. High p_T Particle Spectra

In Run II, PHENIX recorded more than 30 million minimum bias Au+Au events. This event sample enables us to reach 10 GeV/c in the transverse momentum spectra of both identified neutral pions and charged hadrons. In addition, we recorded 140 million p+p events in which we measure neutral pions up to 13 GeV/c. Shown in Fig. 1 is the neutral pion production cross section as a function of p_T , measured with the PbSc, for p+p collisions [4]. The measured p+p spectrum is compared to a fit to UA1 data [5] over the range $p_T < 6$ GeV/c, extrapolated to higher p_T . Although our measurement agrees with the UA1 data, it disagrees with this extrapolation at very high p_T . This new measurement provides an important reference spectrum for comparison with the Au+Au data.

For Au+Au collisions, the events are binned into centrality selections, and the spectra are shown for the most central bin and a peripheral bin in Figs. 2 and 3. Centrality is expressed as a percentage of the total inelastic cross section. In the Run II data, the charged hadron yields are measured up to $p_T = 10$ GeV/c for central events and $p_T = 5$ GeV/c for peripheral events, while the neutral pion yields are measured up to 8 and 6.5 GeV/c for central and peripheral events respectively.

4. R_{AA} for Neutral Pions

The nuclear modification factor quantifies the effect of A+A compared to p+p collisions on particle yields for point-like processes. It is defined as the ratio of the particle yield in a A+A collision to the yield in a p+p collision scaled by the mean number of binary (nucleon+nucleon) collisions N_{coll} in the A+A event sample. Because hard processes are generally believed to scale with N_{coll} (“binary-scaling”), this ratio is expected to be one

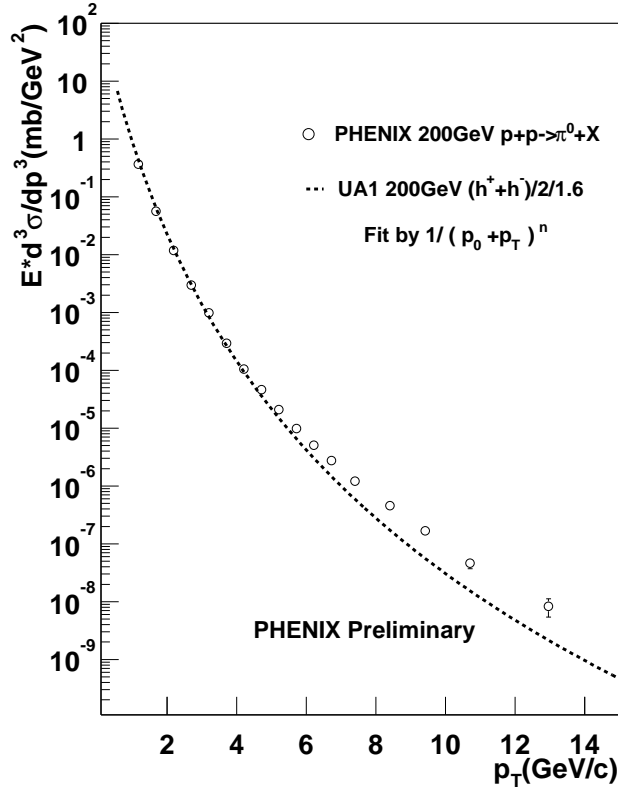


Figure 1. Neutral pion production cross section vs. p_T in p+p collisions at $\sqrt{s_{NN}} = 200$ GeV.

at high p_T in the absence of any nuclear effects.

$$R_{AA}(p_T) = \frac{(\text{Yield per A + A collision})}{\langle N_{coll} \rangle (\text{Yield per p + p collision})} = \frac{d^2 N^{A+A} / dp_T d\eta}{\langle N_{coll} \rangle (d^2 \sigma^{p+p} / dp_T d\eta) / \sigma_{inelastic}^{p+p}}. \quad (1)$$

Shown in Fig. 4 is R_{AA} as a function of p_T for central Pb+Pb collisions at $\sqrt{s_{NN}} = 17$ GeV from WA98 [8] and central Au+Au collisions at $\sqrt{s_{NN}} = 130$ GeV from PHENIX Run I [9]. Already in this comparison, the suppression relative to binary-scaling at 130 GeV is striking. It is quite different from the enhancement observed at 17 GeV. This enhancement is known as the ‘‘Cronin effect’’ [10] and has been attributed to p_T broadening due to initial state scatterings [11, 12]. Figure 5 shows R_{AA} for central and peripheral Au+Au collisions at $\sqrt{s_{NN}} = 200$ GeV. The central data again show a suppression as seen at 130 GeV. With a measurement that extends to much larger p_T , the suppression is shown to persist up to $p_T \sim 8$ GeV/c and is as much as a factor of 5-6 at the largest p_T . The measurement of the p+p reference spectrum with the same detector greatly reduces the systematic error in R_{AA} for central events. The R_{AA} for peripheral events is consistent with binary-scaling (p+p yields scaled by the number of binary collisions in the peripheral event sample). The error in this ratio is dominated by the uncertainty in $\langle N_{coll} \rangle$ for peripheral collisions. Within the rather large errors, the spectrum for peripheral collisions does not show effects of the nuclear medium. If there is a Cronin effect at RHIC, it is not strongly evident in peripheral collisions.

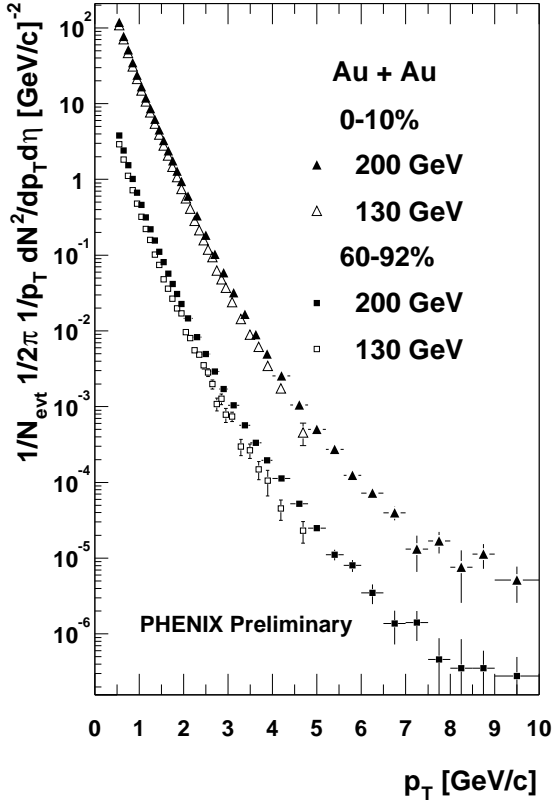


Figure 2. Invariant yields of $(h^+ + h^-)/2$ as a function of p_T in Au+Au collisions at $\sqrt{s_{NN}} = 200$ GeV [6] and 130 GeV for centrality selections of 0-10% and 60-92%.

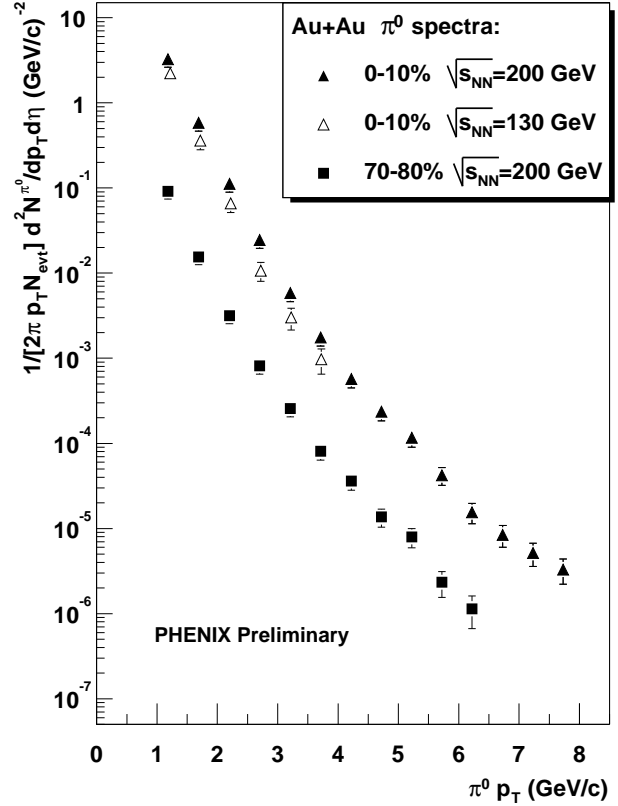


Figure 3. Invariant yields of π^0 as a function of p_T in Au+Au collisions at $\sqrt{s_{NN}} = 200$ GeV and 130 GeV for centrality 0-10% and $\sqrt{s_{NN}} = 200$ GeV for centrality 70-80%.

There are a number of model predictions, shown in Fig. 6, that were made prior to the release of the Run II data. In the case of one model which assumes energy loss that is constant with respect to the parton's energy [12], R_{AA} increases by a factor of ~ 2 from $p_T \sim 3.5$ to $p_T \sim 8$ GeV/c. Although the magnitude of the suppression qualitatively describes the data at $p_T \sim 4$ GeV/c, the increasing R_{AA} with p_T is contrary to what is observed in central Au+Au collisions. Two other models which use a common formalism for including energy-dependent energy loss differ in the point where the calculation is begun (thus resulting in somewhat different predictions). One such model predicts an R_{AA} that increases only slightly with increasing p_T [13], while another model predicts a nearly constant R_{AA} from $p_T \sim 4$ to at least $p_T \sim 10$ GeV/c [14]. The energy-dependent energy loss models give reasonable agreement with the data. This is also seen in another calculation made subsequent to the release of the Run II data [15].

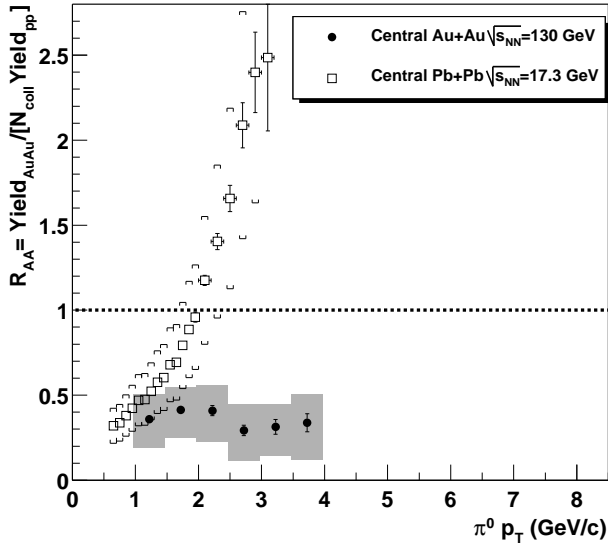


Figure 4. $R_{AA}(\pi^0)$ for central Pb+Pb collisions at $\sqrt{s_{NN}} = 17$ GeV and central Au+Au collisions at $\sqrt{s_{NN}} = 130$ GeV. The error bars are the statistical $\oplus p_T$ -dependent systematic errors. The brackets/boxes are the errors on the normalization of this ratio.

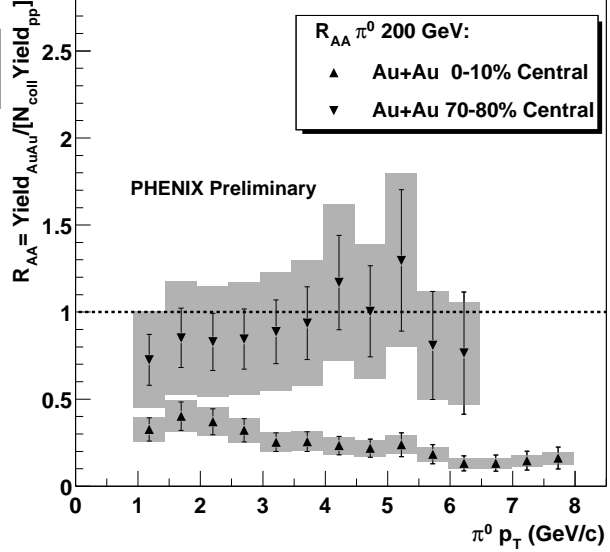


Figure 5. $R_{AA}(\pi^0)$ for central and peripheral Au+Au collisions at $\sqrt{s_{NN}} = 200$ GeV. The error bars are the statistical $\oplus p_T$ -dependent systematic errors. The shaded boxes are the errors on the normalization of the ratio.

5. Comparison of Central Collisions with Respect to Peripheral Collisions

An alternate measure of the nuclear modification is the central-to-peripheral ratio scaled by the number of binary collisions,

$$\text{Binary-Scaled Central/Peripheral} = \frac{\langle \text{Yield per central collision} \rangle / \langle N_{\text{coll}}^{\text{central}} \rangle}{\langle \text{Yield per peripheral collision} \rangle / \langle N_{\text{coll}}^{\text{peripheral}} \rangle}. \quad (2)$$

Since the π^0 spectrum in peripheral Au+Au collisions is consistent with the binary-scaled p+p π^0 spectrum (Fig. 5), this ratio is similar to R_{AA} . An advantage of this ratio is that many of the systematic uncertainties in the measurement cancel, particularly for charged hadrons. A disadvantage is that it is sensitive to the centrality dependence of the Cronin effect, which is not known. Figure 7 shows this ratio as a function of p_T for neutral pions, charged hadrons, and charged pions. The suppression is observed in all three measurements. In the charged hadrons, the suppression factor reaches 3-4 at high p_T . The difference in this ratio between the identified pions and charged hadrons seems to be due to the particle composition. In particular, we find that $p/\pi^0 \sim 1$ in central collisions for $p_T = 2 - 4$ GeV/c while $p/\pi^0 \sim 0.4$ in peripheral collisions [16]. The error in the normalization, denoted by a shaded area for the charged hadrons and outlines for the neutral pions, is dominated by the uncertainty in $\langle N_{\text{coll}} \rangle$ for peripheral collisions.

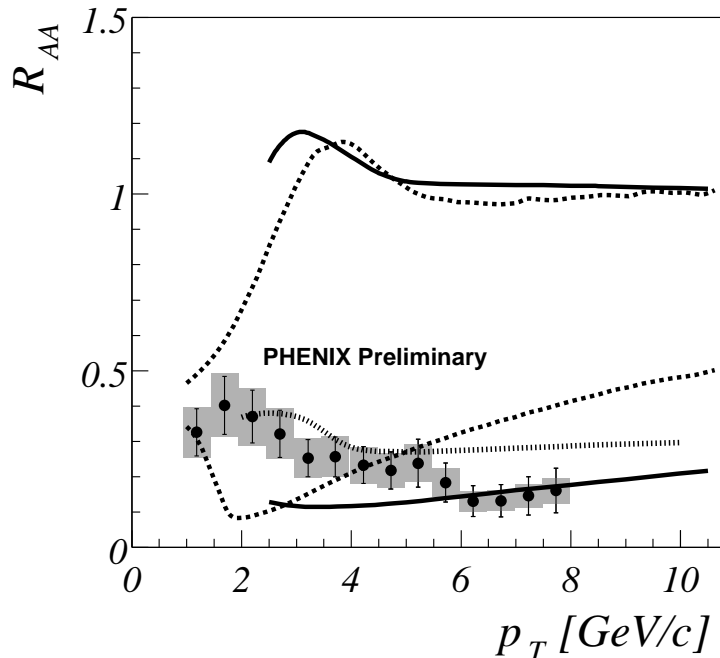


Figure 6. R_{AA} as a function of p_T compared to theoretical predictions for central Au+Au collisions at $\sqrt{s_{NN}} = 200$ GeV. The dotted lines are predictions with and without energy loss (constant) [12]. The solid lines are again predictions with and without energy loss (energy-dependent) [13], and the hashed line is also a prediction with energy-dependent energy loss [14].

6. Centrality Dependence of R_{AA}

As shown in Fig. 5, the 10% most central events have a suppression factor reaching 5-6, while the 70-80% centrality selection is consistent with binary-scaled p+p collisions. We now address the evolution of the nuclear modification factor from the most peripheral to the most central collisions, in terms of the mean number of participating nucleons N_{part} in a centrality selection. For the 10% most central collisions, $\langle N_{part} \rangle = 327$, and for the 70-80% central collisions, $\langle N_{part} \rangle = 14$. Figure 8 shows R_{AA} vs. N_{part} for neutral pions with $4 < p_T < 6$ GeV/c. The suppression gradually increases from peripheral to central events. The same trend is seen in the charged hadron yields. Figure 9 shows the integrated yield scaled by N_{coll} vs. N_{part} for charged hadrons. This quantity is similar to R_{AA} , differing only in normalization by the p+p reference yields. Again the binary-scaled yield decreases, or the suppression increases, gradually with increasing N_{part} .

7. Particle Composition at High p_T

PHENIX can measure the p/π ratio up to almost 4 GeV/c in p_T [16], at which point protons can no longer be distinguished from other particles via their time of flight. Since neutral pions are identified to much higher p_T , we can look at the ratio of π^0 to nonidentified charged hadrons $(h^+ + h^-)/2$ for $p_T > 4$ GeV/c. This ratio is shown in Fig. 10 for minimum bias events. The surprising feature that this ratio does not increase for trans-

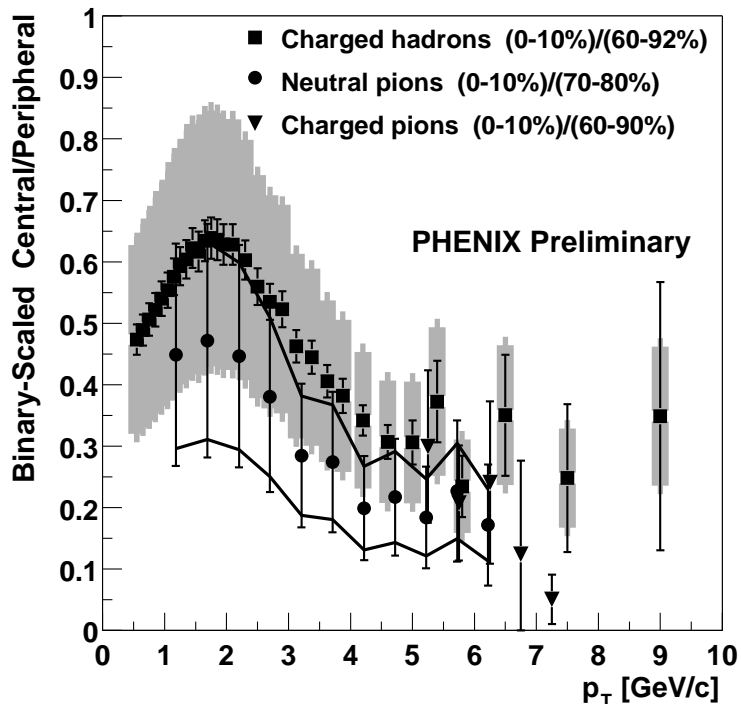


Figure 7. Binary-scaled central-to-peripheral ratio vs. p_T for charged hadrons, neutral pions, and charged pions measured in Au+Au collisions. The error bars are statistical \oplus p_T -dependent systematic errors. The error in the overall normalization is shown as outlines for neutral pions and a shaded area for charged hadrons. For charged pions, the error is dominated by statistics.

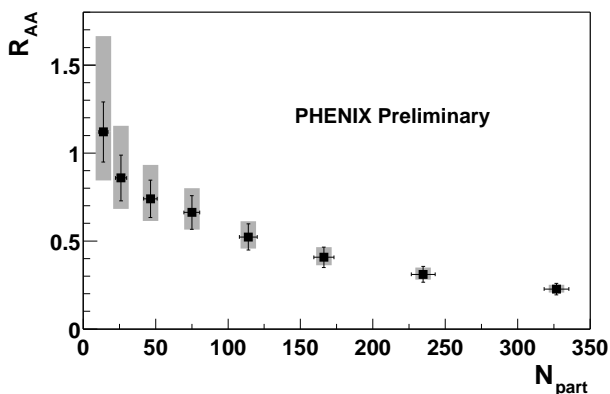


Figure 8. R_{AA} vs. N_{part} (or centrality of the collision) for neutral pions with $4 < p_T < 6$ GeV/c. The shaded boxes denote the error on $\langle N_{coll} \rangle$. There is an additional error of 20% in the overall normalization that is not shown.

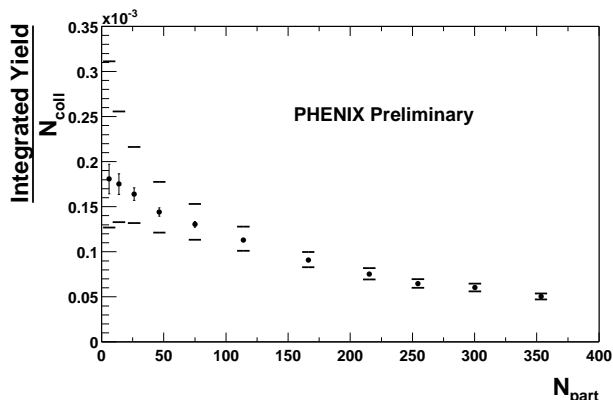


Figure 9. Integrated yield scaled by N_{coll} vs. N_{part} for charged hadrons with $p_T > 4$ GeV/c. The brackets denote the error on $\langle N_{coll} \rangle$.

verse momenta greater than 4 GeV/c, but remains nearly constant at a value around 0.5, indicates that approximately half of the charged hadrons at high p_T are protons and/or kaons, assuming $\pi^0 = (\pi^+ + \pi^-)/2$. This result is rather different from hard processes as measured in e^+e^- collisions [17]. The interpretation for this new result is not yet clear. There may be some other production mechanism for protons and/or kaons in Au+Au collisions at these large transverse momenta. Alternatively, the large proton and/or kaon content at high p_T could be due to a difference in the suppression of pions relative to protons/kaons.

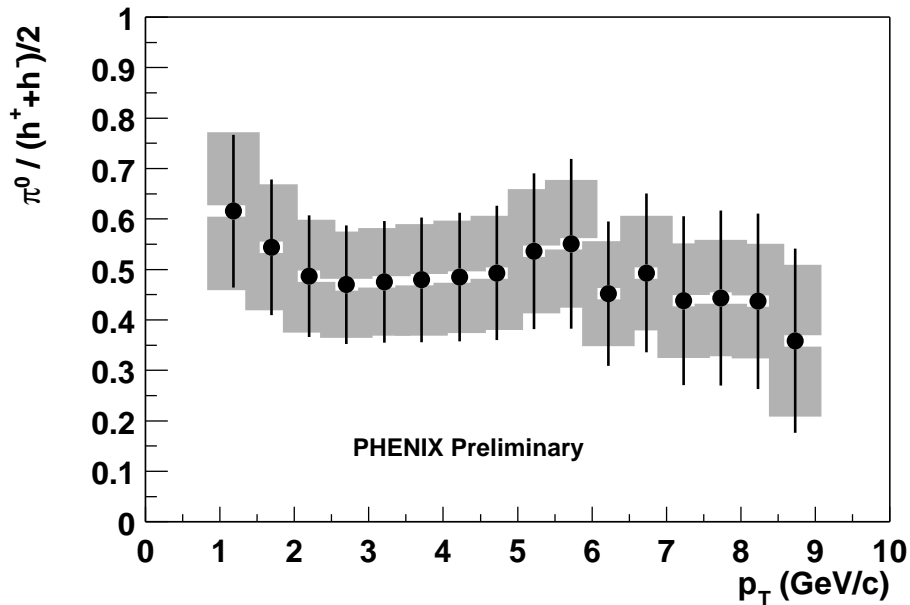


Figure 10. Ratio of π^0 to $(h^+ + h^-)/2$ as a function of p_T for minimum bias Au+Au collisions.

8. Evidence for Jets

Since jets cannot be directly observed in a Au+Au collisions, a correlation analysis is required to detect their presence. We take a high p_T neutral particle, a cluster in the EMCAL with energy greater than 2.5 GeV, as the trigger and correlate it with all charged particles in the event within a given range in p_T . Comparing the correlations that we measure in p+p collisions at $\sqrt{s_{NN}} = 200$ GeV to those from the PYTHIA event generator [18], we establish that PYTHIA reproduces the behavior of jets known to be present in p+p collisions. PYTHIA is then compared to Au+Au collisions at $\sqrt{s_{NN}} = 200$ GeV, which demonstrates that the correlations we observe in Au+Au collisions behave as expected for jets, both in the azimuthal and polar angles. Figure 11 shows the background-subtracted correlation in the azimuthal angle $\Delta\phi$ of the trigger particle with charged particles having p_T between 2 and 4 GeV/c. Also shown is a fit to the data of the correlation produced by PYTHIA with an added $\cos(2\phi)$ term. The $\cos(2\phi)$ term accounts for the contribution of flow to the correlation, while the coefficient of the PYTHIA term represents the

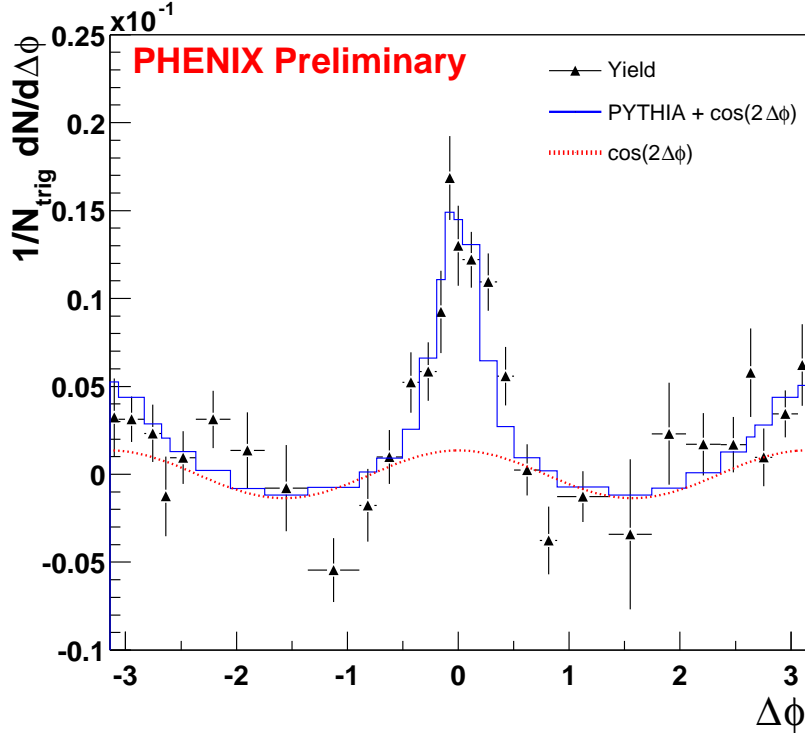


Figure 11. Acceptance-corrected yield (in 20-40% centrality selection) fit to PYTHIA plus an elliptic flow term.

contribution due to jets. Further details of this analysis are given elsewhere [19]. From the figure, one can see that much of the correlation can be attributed to jets (PYTHIA), particularly the near-side correlation around $\Delta\phi = 0$. The trigger particle is typically a photon from a π^0 decay. This is strong evidence that when we trigger on a high p_T π^0 , we are indeed looking at a leading particle from a jet.

9. Conclusions

We have presented p_T spectra for charged hadrons in Au+Au collisions and neutral pions in Au+Au and p+p collisions and have shown that the high p_T suppression observed in Run I RHIC data at $\sqrt{s_{NN}} = 130$ GeV [9, 20] persists up to $p_T \sim 8$ GeV/c at $\sqrt{s_{NN}} = 200$ GeV. The neutral pions are suppressed by a factor of 5-6 and the charged hadrons by 3-4 for $p_T > 4$ GeV/c in the most central collisions. The suppression increases gradually with increasing centrality, or N_{part} . We have also shown that when triggering on a high p_T neutral particle, which is predominantly a photon from a π^0 decay, the correlation between the neutral and charged particles in the event is jet-like. This is strong evidence that the neutral pions that we measure at high p_T indeed have significant contributions from jet fragmentation. Finally, we have shown that approximately half of the charged hadrons at high p_T are not pions, but protons and/or kaons, up to $p_T \sim 9$ GeV/c.

REFERENCES

1. J.F. Owens *et al.*, Phys. Rev. **D18**, 1501 (1978).

2. M. Gyulassy and M. Plümer, Phys. Lett. **B243**, 432 (1990); R. Baier *et al.*, Phys. Lett. **B345**, 277 (1995); X.N. Wang and M. Gyulassy, Phys. Rev. Lett. **68**, 1480 (1992); X.N. Wang, Phys. Rev. **C58**, 2321 (1998).
3. PHENIX Collaboration, D. Morrison, *et al.*, Nucl. Phys. **A638**, 565c (1998); PHENIX Collaboration, W. Zajc, *et al.*, Quark Matter 2001.
4. H. Torii for the PHENIX Collaboration, these proceedings.
5. C. Albajar *et al.*, Nucl. Phys. **B335**, 261 (1990).
6. J. Jia for the PHENIX Collaboration, these proceedings.
7. D. D'Enterria for the PHENIX Collaboration, these proceedings.
8. M.M. Aggarwal *et al.* [WA98 Collaboration], Eur. Phys. J. C23 (2002) 225-236.
9. K. Adcox *et al.* [PHENIX Collaboration], Phys. Rev. Lett. **88**, 022301 (2002).
10. D. Antreasyan *et al.*, Phys. Rev. **D19**, 764 (1979).
11. M. Lev and B. Petersson, Z. Phys. **C21**, 155 (1983); T. Ochiai *et al.*, Prog. Theor. Phys. 75, **288** (1986).
12. X.N. Wang, Phys. Rev. C61, 064910 (2000).
13. P. Levai *et al.*, Nuclear Physics A698 (2002) 631.
14. I. Vitev and M. Gyulassy, these proceedings, hep-ph/0208108; M. Gyulassy, P. Levai and I. Vitev, Nucl. Phys. B 594, p. 371 (2001).
15. S. Jeon, J. Jalilian-Marian and I. Sarcevic, nucl-th/0208012.
16. T. Sakaguchi for the PHENIX Collaboration, these proceedings.
17. P. Abreu *et al.* [DELPHI Collaboration], Eur. Phys. J. C17, 207 (2000), DOI 10.1007/s100520000449.
18. T. Sjostrand, Comput. Phys. Commun. **82**, 74 (1994).
19. M. Chiu for the PHENIX Collaboration, these proceedings.
20. C. Adler *et al.* [STAR Collaboration], nucl-ex/0206011.